Supporting Information

Smart Building Block with Colored Radiative Cooling Devices and Quantum Dot Light Emitting Diodes

Sang Yeop Lee[a], Dongwoo Chae[a], Jungho Kim[b], Seongkeun Oh[a], Hangyu Lim[a], Jiwan Kim[b]*, Heon Lee[a]*, and Soong Ju Oh[a]*

Evaluation of RC performance

The cooling power, $P_{cooling}$ was calculated based on the following energy balance equation:

$$P_{cooling}(T,T_{amb}) = P_{rad}(T) - P_{amb}(T_{amb}) - P_{solar} - P_{non-rad}(T,T_{amb}), (1)$$

where

$$P_{rad}(T) = \int_0^{2\pi}\int_0^{\frac{\pi}{2}}\int_0^{\infty} I_{BB}(T,\lambda)\varepsilon(\lambda,\theta)cos\theta sin\theta d\lambda d\theta d\varphi, (2)$$

indicates the power with thermal radiation of the surface of the object and

$$P_{amb}(T_{amb}) = \int_0^{2\pi}\int_0^{\frac{\pi}{2}}\int_0^{\infty} I_{BB}(T_{amb},\lambda)\varepsilon(\lambda,\theta)\varepsilon_{amb}(\lambda,\theta)cos\theta sin\theta d\lambda d\theta d\varphi, (3)$$

denotes the power loss from the object's absorption of atmospheric emission.

$$P_{solar} = \int_0^{\infty} I_{solar}(\lambda)\varepsilon(\lambda,\theta)d\lambda, (4)$$

represents the power loss by the object's solar absorption.

$$P_{non-rad}(T,T_{amb}) = h_c(T_{amb} - T), (5)$$

expresses the power loss caused by nonradiative conduction and convection.

Here, I_{BB}, $\varepsilon_{atm}(\lambda,\theta)$, h, c, k_B, I_{solar} represent blackbody radiation density, spectral emissivity of the atmosphere, Planck's constant, speed of light, Boltzmann constant, and solar power density, respectively. $P_{cooling}(T) > 0$ indicates the subambient cooling of the sample, and $\Delta T_{cooling}$ is calculated using the equation $\Delta T_{cooling} = T - T_{amb}$.

The following equations were used to determine the reflectance (R), transmittance (T), and absorptivity (A) in the solar region (R_{solar}, T_{solar}, and A_{solar}):

$$X_{solar} = \int_{0.3\ \mu m}^{2.5\ \mu m} \frac{I_{solar}(\lambda)X(\lambda)}{I_{solar}(\lambda)} d\lambda, (6)$$

where X denotes reflectance, transmittance, or absorption. The following equation was used to derive the emissivity (ε) in the atmospheric window: [1,2]

$$\varepsilon_{LWIR} = \int_{8\ \mu m}^{13\ \mu m} \frac{I_{BB}(T_{amb},\lambda)\epsilon(\lambda)}{I_{BB}(T_{amb},\lambda)} d\lambda, (7)$$

Fabrication and optical properties of Ag-PDMS and RC paint radiative cooling device

An Ag-PDMS radiative cooling device uses an Ag film deposited by thermal evaporation as a reflector for visible light and coated with a 100 µm PDMS layer on top of it to increase absorption and emission efficiency in the mid-infrared range (Figure s1a). In the case of an RC paint cooling device, RC paint can be used instead of Ag and PDMS. The RC paint was applied to a glass substrate. The visible light absorption of the produced Ag-PDMS and RC paint cooling devices was measured using UV-vis spectroscopy (Figure s2a). We confirmed that the RC paint had a low absorption rate of 0.21% at 550 nm under visible light and a very low absorption rate of less than 1% over the entire range of 400–800 nm, thereby effectively preventing solar heating. The absorption rate of the Ag-PDMS cooling device was 3.14% at 550 nm and increased as it approached 400 nm, measuring 8.56% at 400 nm. The absorption rate and emission efficiency in the mid-infrared range were measured using Fourier-transform infrared (FT-IR) spectroscopy (Figure s2b). The Ag-PDMS cooling device and RC paint cooling device had very high absorption rates of over 80% in the range of 8–13 µm, indicating that effective heat exchange with space could occur.

Supplementary Figures

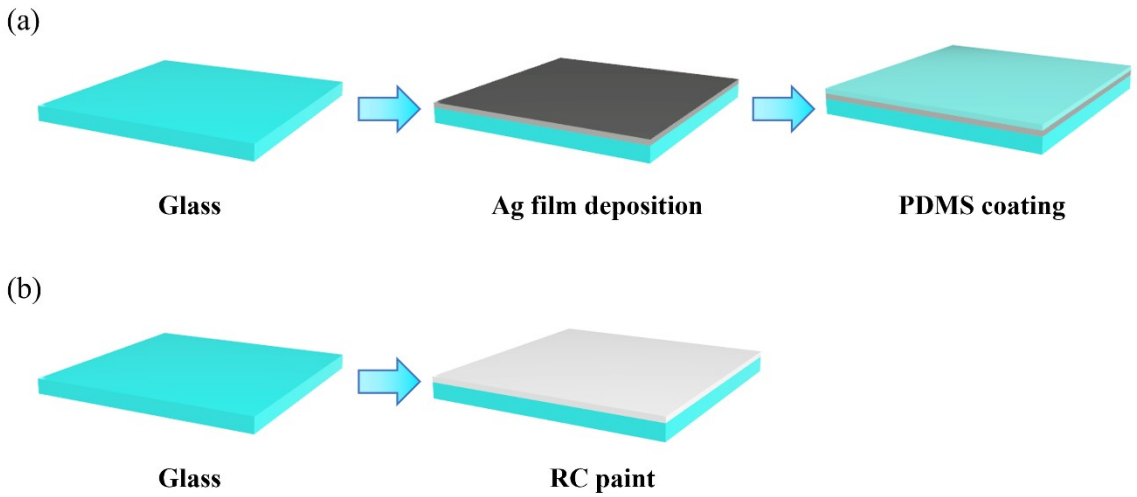

Figure S1. (a) Fabrication process of Ag-PDMS radiative cooling device. (b) Fabrication process of RC paint radiative cooling device.

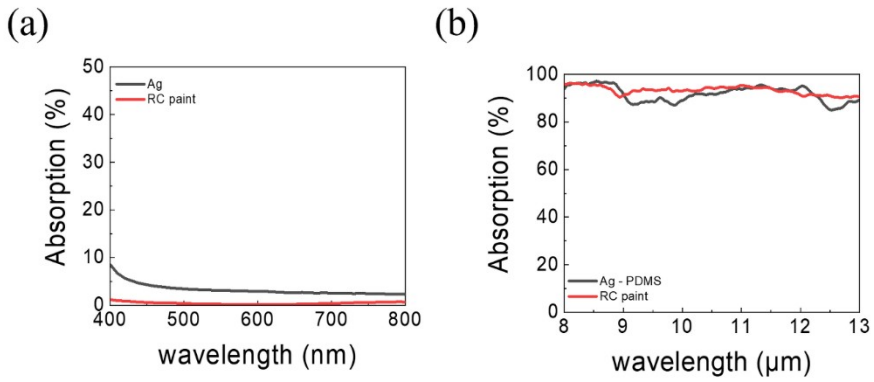

Figure S2. (a) UV-vis spectra of Ag-PDMS and RC paint radiative cooling devices. (b) FT-IR spectra of Ag-PDMS and RC paint radiative cooling devices.

Figure S3. Image of the synthesized CdZnSeS/ZnS core-shell nanocrystals under white light (left) and UV light (right).

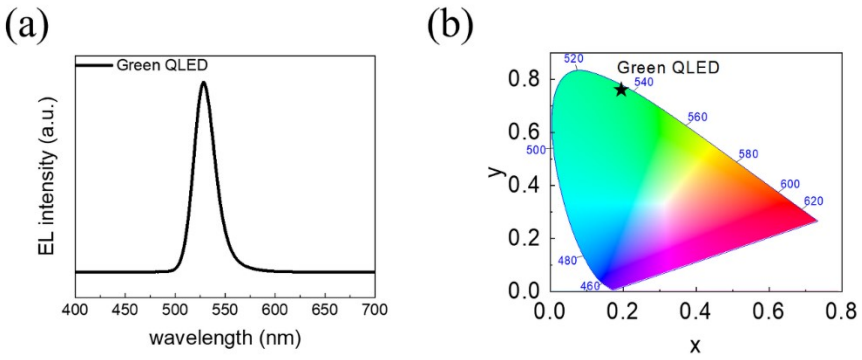

Figure S4. (a) Electroluminescence spectra of the fabricated inverted QLED. (b) CIE 1931 color coordinate of the fabricated inverted QLED.

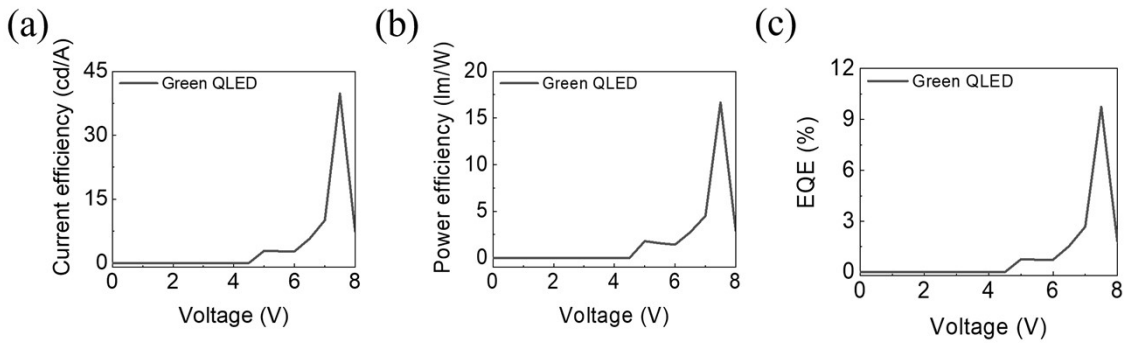

Figure S5. (a) Current efficiency of the fabricated inverted QLED. (b) Power efficiency of the fabricated inverted QLED. (c) External quantum efficiency of the fabricated inverted QLED.

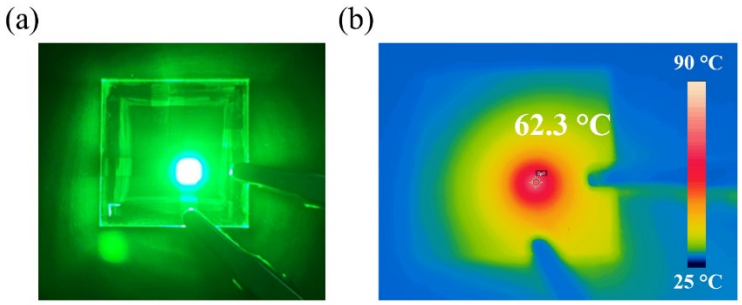

Figure S6. (a) Image of the maximum brightness of an inverted QLED at 7.5 V. (b) Infrared image of the maximum temperature of an inverted QLED at 7.5 V.

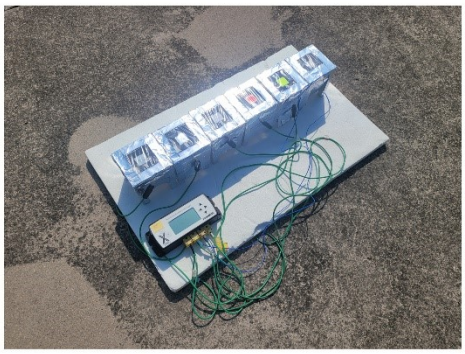

Figure S7. Image of the equipment for the outdoor measurement of the cooling performance.

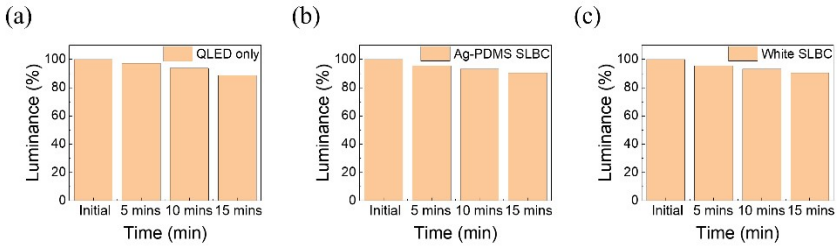

Figure S8. (a) Reductions in the luminances of the QLED-only device and the (b) Ag-PDMS and (c) white SLBCs.

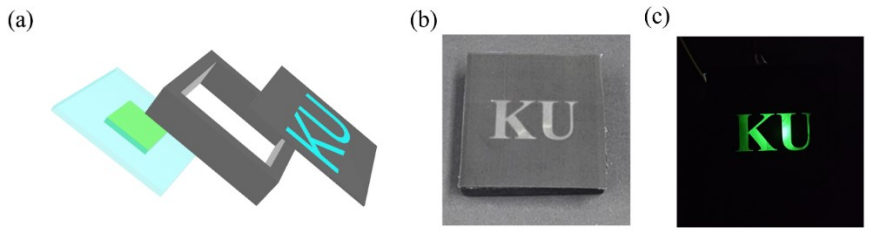

Figure S9. (a) Schematic of imitation SLBC billboard. (b) Image of imitation SLBC billboard. (c) Image of imitation SLBC billboard under 6 V.

References

1 A. P. Raman, M. A. Anoma, L. Zhu, E. Rephaeli and S. Fan, *Nature*, 2014, **515**, 540–544.

2 J. Mandal, Y. Fu, A. C. Overvig, M. Jia, K. Sun, N. N. Shi, H. Zhou, X. Xiao, N. Yu and Y. Yang, *Science*, 2018, **362**, 315–319.